Preprint, 2019

Published 26 November 2019
International Journal of Modern Physics A
Vol. 34, No. 36 (2019) 1942008 (14 pages)
DOI: 10.1142/S0217751X19420089

Muon loss rates from betatron resonances at the Muon *g*-2 Storage Ring at Fermilab*

D. A. Tarazona†, M. Berz and K. Makino
Department of Physics and Astronomy,
Michigan State University,
220 Trowbridge Road
East Lansing, MI 48824, USA

Received 5 February 2019
Revised 6 May 2019
Accepted 6 May 2019

The Muon *g*-2 Experiment at Fermilab (E989) is directed toward measuring the muon magnetic anomaly, $a_\mu = (g-2)/2$, with total statistical and systematic errors of 0.14 ppm. This new measurement will serve as strong probe of effects of as yet undiscovered particles beyond the Standard Model (SM), and perhaps validate or disprove other theoretical models beyond the SM. Of special interest is the reduction of muon losses from the storage ring to achieve the precision needed at the Muon *g*-2 Experiment. For this purpose, we have developed a detailed and precise symplectic model of the Muon *g*-2 Storage Ring using *COSY INFINITY* that considers measured inhomogeneities of the magnetic field; high-order representation of the Electrostatic Quadrupole System (EQS) electrostatic field at different stages of the experiment including fringe fields; injection to the ring based on measurements; and beam collimation. Specifically, we have performed numerical analyses of the rate of muons that are lost before they have a chance to decay for several possible configurations of the EQS in order to find the best possible scenarios that minimize muon losses and understand the resonance mechanisms that contribute to betatron and possibly spin resonances. Additionally, comparisons with measurements have permitted the determination of whether observed resonances come from anticipated features of the *g*-2 storage ring or from unexpected sources of error whose effect could be detrimental to the precision of E989.

Keywords: Muon *g*-2 Experiment; simulation; storage ring; muon beam; electrostatic quadrupole; beam collimator; betatron resonance; *COSY INFINITY*.

1. Introduction

The experimental anomaly a_μ that the Muon *g*-2 Experiment at Fermilab (E989) aims to measure is extracted from

$$a_\mu = \frac{g_e}{2}\frac{\omega_a}{\omega_p}\frac{m_\mu}{m_e}\frac{\mu_p}{\mu_e}, \tag{1}$$

*Fermilab report: FERMILAB-CONF-19-021-AD
†Email: tarazona@msu.edu. ORCID: 0000-0002-7823-7986.

where g_e is the electron g-factor; ω_a the spin precession frequency in the horizontal midplane relative to the momentum direction of muons[a] inside the storage ring; ω_p the Larmor frequency of a free proton; m_μ and m_e the muon and electron masses, respectively; and μ_p, μ_e are the proton and electron magnetic dipole moments.[1] To hold the equality in Eq. 1 sufficiently for the purposes of E989, the two measured frequencies ω_a and ω_p must be determined to high precision; in regard to the systematic error of ω_a, it is expected to be $\delta\omega_a^{sys} < 70$ ppb. One of the largest contributors to $\delta\omega_a^{sys}$ comes from muons being lost before they decay. Such losses are mainly a consequence of muons hitting the collimators centered around the beam orbit due to nonlinearities in the motion and are significantly increased when configurations of the ring approach betatron resonances. Muons that escape the ring before they decay are referred to as "lost muons."

Muon losses contribute to the systematics of E989 by introducing distortions to the overall beam spin precession frequency $\langle\omega_a\rangle = \langle d\varphi_a/dt\rangle$: correlations between spin coordinates and dynamical variables of lost muons might lead to shifts of the expected $\langle\omega_a\rangle$. This can take place if, for instance, muons within a certain momentum range are preferentially lost during data taking and, at the same time, the muon beam injected into the storage ring has spin-momentum correlations previously developed along the beam delivery system of E989.[2] If the lost muon fraction is minimized, the associated systematic effect can be reduced, too.

Beam dynamics simulations of lost muons at the g-2 storage ring have been performed using *COSY INFINITY*.[3] In particular, preparation of detailed high-order transfer maps calculated with Differential Algebraic (DA) methods yield precise solutions of the beam optics ordinary differential equations (ODEs) that cover nonlinearities associated to the small but relevant imperfections of E989. The use of transfer maps in *COSY INFINITY* permits fast particle tracking in contrast with conventional orbit-integration beam dynamics codes. These features are essential for detailed and high-statistics studies of the muon beam in the g-2 storage ring, which encompass high-order electric and magnetic multipole terms from the Electrostatic Quadrupole System (EQS) design and measured magnetic field imperfections, respectively. Additionally, storage ring simulations utilize *COSY INFINITY*'s rigorous and highly accurate treatment of fringe fields and effective field boundaries for the EQS and accounts for beam collimation during the scraping, transition, and production stages of the experiment. Symplectification is performed using *COSY INFINITY*'s most accurate symplectification method (EXPO).[4]

In the following sections, we first describe the g-2 storage ring *COSY*-based model. Then, results of muon loss rates simulations across a wide range of operational points are discussed, whose purposes are to: identify the running conditions that minimize muon losses; and distinguish the particular resonant conditions that excite muon loss rates, for which several scenarios of the guide fields within the ring

[a]It is customary to dub anti-muons (μ^+) as "muons" in the Muon g-2 Collaboration. We adopt the same convention throughout this paper.

are analyzed.

2. Storage Ring Model

A muon beam enters the storage ring through a hole in the back-leg of the C-shaped magnet that guides the magnetic field induced by currents in superconducting coils to the storage region.[1] The time-dependent injection kick produced by the kicker magnet – located about 90° from the exit of the hole (see Fig. 1) and meant to improve alignment of the injected beam with the reference orbit[5] – is included in our model, altogether with the EQS to focus the beam vertically and the small but relevant inhomogeneities of the vertical magnetic field. The essential components of the storage ring simulation are described in this section.

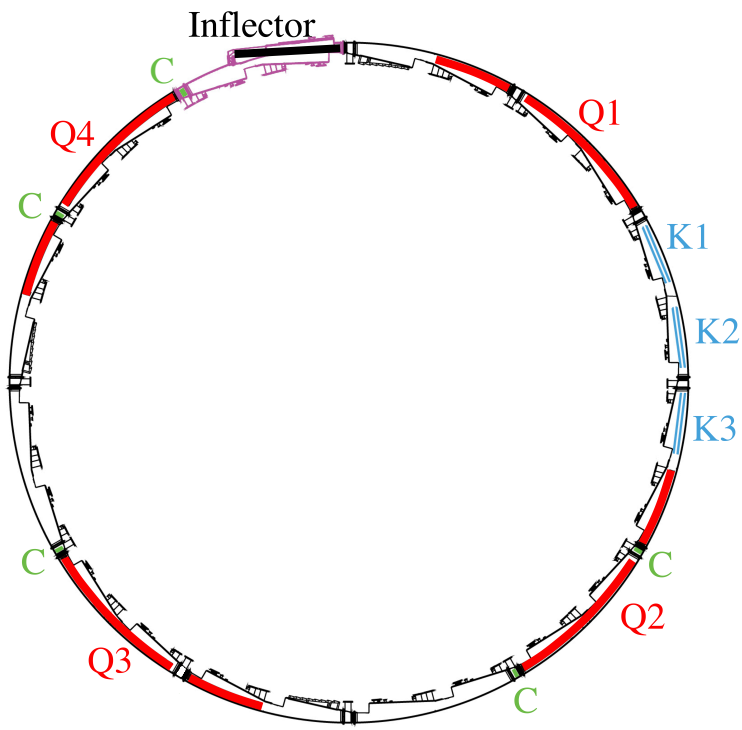

Fig. 1. Layout of the Muon g-2 storage ring at Fermilab.[6] The four locations of the EQS are next to labels "Q1-Q4" (each covering 39° azimuthally) and labels "K1-K3" indicate the place of the injection kicker plates within the ring. "C" labels denote the beam collimators arrangement.

2.1. *Initial Distribution*

The initial conditions of the beam injected to the storage ring are taken from a *BMAD* simulation[6] that transfers the beam distribution at the entrance of the ring, which was previously calculated with *G4BEAMLINE*[7] and validated by independent *BMAD*[8] and *COSY*[2] based simulations of the beam delivery system at E989. The distribution is transferred through the material-free yoke volume where a superconducting inflector is placed to cancel out the field. At this point, the mismatched beam is centered 75 mm radially outward from the ideal orbit. The beam initial time profile – important for the injection kicking process – is set based on measurements from scintillating detectors (see Fig. 2).

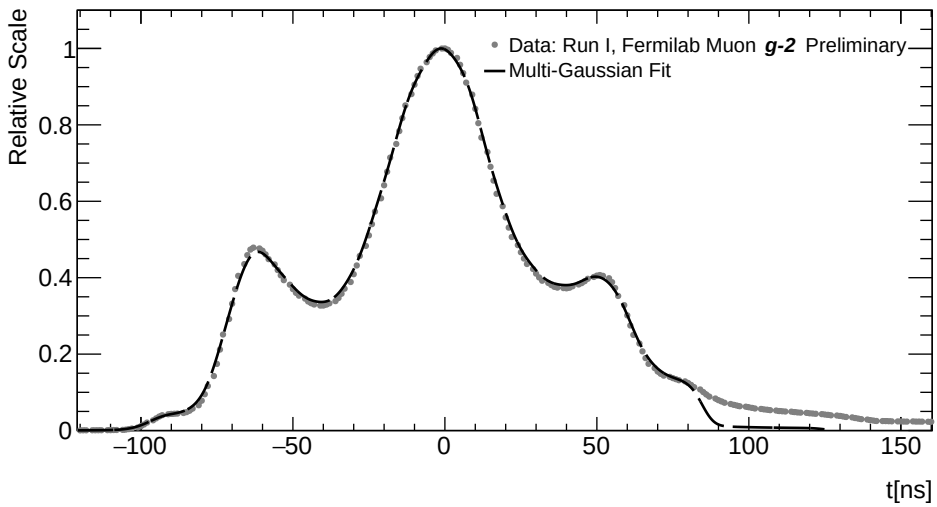

Fig. 2. Normalized beam time distribution sample at injection. The time profile of the injected beam implemented in *COSY*-based ring model simulations (black dashed curve) was obtained from an interpolation to the experimental data[6] (gray dots).

On the one hand, about 3% of the injected beam downstream the inflector exit gets stored in simulations after its passage through the injection kicker and the EQS in scraping mode (see 2.5). On the other hand, the fraction of lost muons at later times away from betatron resonances is approximately 0.1% during 66 μs. Thus, to reach enough sensitivity in lost muon simulations, it was needed to artificially inflate the number muons from the *BMAD* simulation. For this purpose, the coordinates of extra initial muons were randomly created within the uniform range $(-\sigma_i/10, \sigma_i/10)$ around each of the original muons coordinates, where σ_i is the beam standard deviation of each coordinate. This technique was found to preserve the averages, standard deviations, and correlations of the original distribution within 3%, 1% and 5%, respectively.

2.2. *Injection Kicker*

The ideal kick would act at a constant field during the time it takes for the front and rear edges of the beam to cross the kicker plates, providing a bend of ∼10.8 mrad radially outward. However, during initial operations of E989 the kicker exhibited a ringing pattern of oscillatory voltages similar in shape to the illustration shown in Fig. 3, which we added into our model.[9] In our simulations, the kick – proportional in strength to the pattern in Fig. 3 – is instantaneously applied to each particle at the azimuthal center of the kicker.

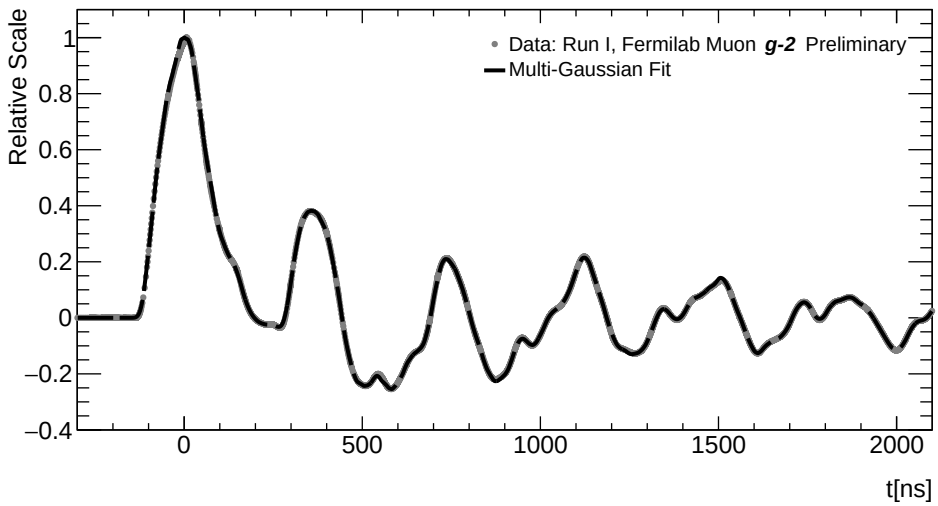

Fig. 3. Normalized kicker pulse pattern sample during initial runs. The kicker pulse implemented in simulations (black dashed curve) was obtained from an interpolation of the kicker's measured time-dependent strength[6] (gray dots).

2.3. *Electrostatic Quadrupole System (EQS)*

The EQS is a four-fold azimuthally symmetric system (see Fig. 1) with four plates centered around the ideal orbit[10] meant to supply vertical beam focusing, but at the cost of horizontal defocusing and nonlinear beam dynamics effects due to the specific geometry of the plates. Fully-Maxwellian main fields calculated using conformal mapping[11] are implemented to describe the electric fields generated by the EQS. Fringe fields and the effective field boundary are also modeled based on numerical calculations performed with *COULOMB* (see Ref. 11). These fields consist of 2D electrostatic quadrupole and nonlinear multipole terms that define the potential in the midplane and – as a result of midplane symmetry— are expanded using DA methods[12] to the full spatial dimensions of the curvilinear system superimposed with the vertical magnetic field of the storage ring. The high voltage applied to the

EQS distributes unequally across the aforementioned multipole terms due to the flat design of the electrodes; as a consequence, the quadrupole term —which defines the betatron tunes of the ring – is about 3.4% higher than the voltage applied to the plates (see Ref. 11).

2.4. *Magnetic Field*

The subtle imperfections of the magnetic field within the storage region of the ring drive higher muon losses rates at specific high voltage settings of the EQS. In our model, we include such inhomogeneities based on fits of nuclear magnetic resonance (NMR) measurements.[6] The azimuth-independent fits provide 2D magnetic normal and skew multipole terms (up to the decapole term) whose strengths vary along the azimuth of the ring. Due to the inability of NMR probes to measure the magnetic field direction, radial and vertical fields are fully degenerate; the 2D fits take the vertical direction as reference and the radial dipole field is captured in simulations from measurements performed with a Hall probe.[6]

With continuous functions made of superimposed Gaussians, we model each measured multipole and apply symplectic kicks separated by $\sim 0.1^\circ$ proportional to these functions. At each step, the midplane field information for the multipoles is used in *COSY* to automatically reconstruct the out-of-plane information from Maxwell's equations.[12]

2.5. *Scraping Stage and Beam Collimation*

We simulate $\sim$7.5 μs (i.e. 50 revolutions) of scraping stage after beam injection, where some EQS plates are mis-powered to create closed orbit distortions (see Ref. 10) such that the outermost muons are taken away before data taking. For this purpose, the field that corresponds to the mis-powered plate has been also calculated with conformal maps (see Ref. 11) and is superimposed to the main field of the EQS. Thereafter, a series of transfer maps is calculated to recreate the exponential transitioning of mis-powered EQS plates back to the nominal high voltage value. After 37.2 μs, the mis-powered plates voltage is returned to the nominal value and symplectic tracking is performed during 150 μs (i.e. 1,000 revolutions).

Five collimators are placed around the ideal closed orbit in our numerical studies to resemble the design configuration of the collimation system (see Fig. 1), whose purpose is to minimize muon losses by cleaning the muon beam before E989 production data taking.

To validate the storage ring simulation model, we compare simulation results with measured betatron tunes (Table 1) and relative decay positron storage[13] (Fig. 5) for several EQS high voltage (HV) configurations.

In Table 1, relative differences between measured[6] and simulated horizontal, ν_x, and vertical, ν_y, betatron tunes are shown. Experimental tunes are extracted from measurements (preliminary) of the cyclotron and Coherent Betatron Oscillation (CBO) frequencies. The vertical CBO peak from a Fast Fourier Transform (FFT)

Table 1. Comparison of computed tunes with measurements.

HV[kV]	$\lvert\Delta\nu_x/\nu_x\rvert$ [%]	$\lvert\Delta\nu_y/\nu_y\rvert$ [%]
13.0	0.033	0.715
15.0	0.037	0.724
17.6	0.019	0.375
19.0	0.023	0.343
20.2	0.016	0.407
20.5	0.041	0.575

analysis wherefrom the vertical CBO frequency is extracted exhibits a larger uncertainty compared to the horizontal CBO frequency case. This is experimentally explained by a vertical CBO peak not as well defined as the horizontal peak sample, which may be due to vertical nonlinear tune-shifts being larger than the horizontal tune-shifts for the g-2 ring case[14] and/or slowly-varying betatron tunes attributable to unexpected behavior of the EQS, whose effect in the magnitude of the vertical tune is more adverse (see Fig. 4). For these reasons, there is less agreement with computed vertical tunes in Table 1.

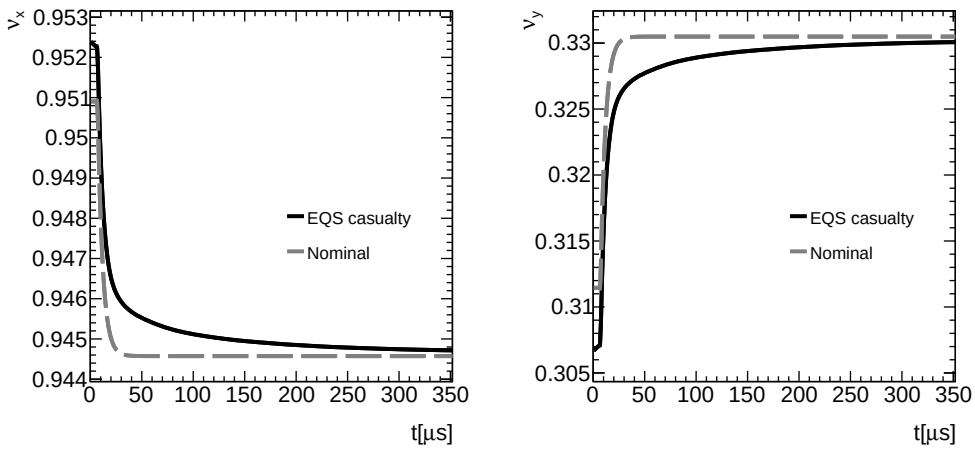

Fig. 4. Horizontal (left) and vertical (right) betatron tunes from the *COSY*-based storage ring model simulations ($HV = 18.3$ kV). The horizontal axis represents time where the beam is injected into the storage ring at approximately 30 μs. At the end of the first production run of E989, the high voltage applied to one of the four sections of the EQS was found to produce an unforeseen electric field due to damaged instrumentation, which was fixed afterwards. Dashed curves correspond to tunes in the nominal case, whereas solid lines depict tunes under the effect of this unforeseen electric field.

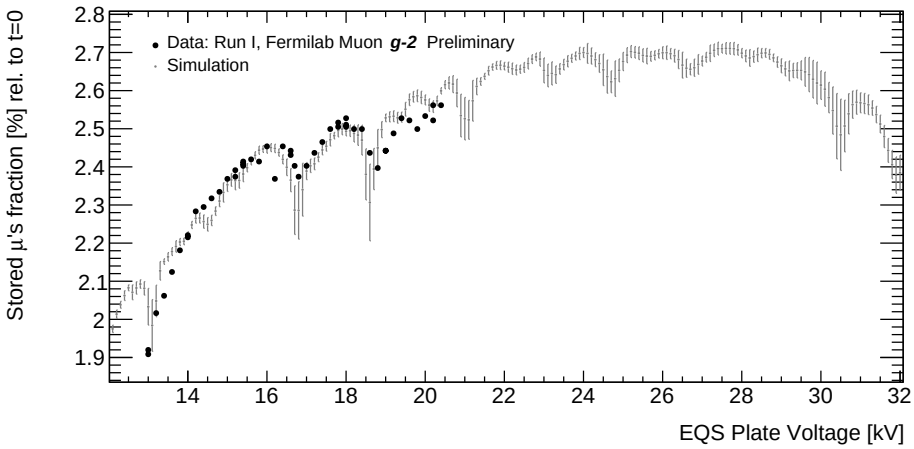

Fig. 5. Qualitative comparison between stored muons rates from simulations (gray) at $t = 186$ μs after beam injection and measured relative positron rates (arbitrary units) from stored muon decays[6] (black). Error bars correspond to standard errors of the multiple numerical analyses for each EQS voltage configuration.

3. Studies of Muon Loss Rates

3.1. *Betatron Resonances*

When the transverse motion of muons couples with the periodicity of local forces in the storage ring, their betatron oscillation amplitudes may grow turn by turn in a way that they hit the collimators or other components around the stored beam. Such muons give up energy to the material they interact with, consequently moving inward and then being lost before they decay. The electrostatic scraping right after beam injection is crucial for removing muons with large betatron amplitudes. However, even muons with initially small betatron amplitudes around unstable motion regions in phase-space could be lost at later times under betatron resonances.

High-statistical numerical studies of muon loss rates were performed to unveil the set of operating points where significant betatron resonances occur. In Fig. 6, simulation results for several high-voltage values applied to the EQS are presented. The figure shows the fraction of lost muons during the time interval $121 - 186\,\mu$s after beam injection. Vertical error bars correspond to the standard error of the multiple simulations executed in parallel that were necessary to surpass the resolution required and clearly distinguish resonance peaks (i.e. $\sim 6.8 \times 10^6$ muons at beam injection).

Due to the sensitivity of E989, even the relatively small effects of high-order resonance conditions are avoided. To describe the interplay between the field imperfections in the storage ring and the resonant conditions, we model the ring as a superposition of a uniform vertical magnetic field and electric quadrupole fields coming from the EQS, where all the extra field from the EQS design and magnetic

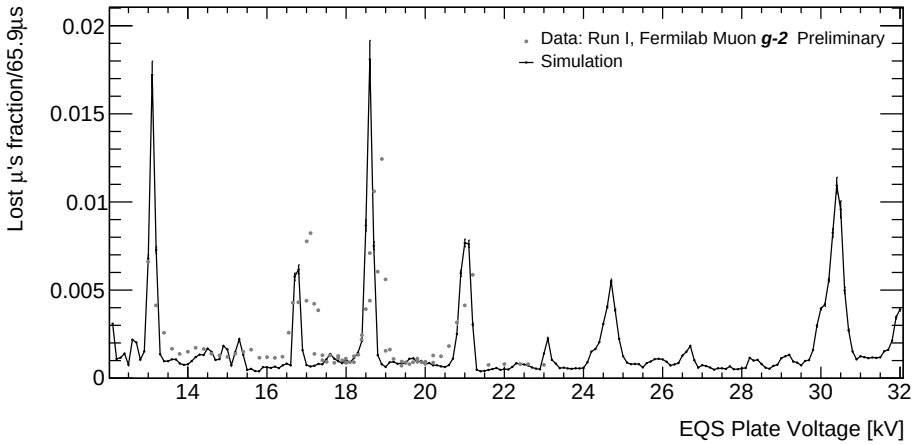

Fig. 6. Fraction of muon losses between $121 - 186$ μs after beam injection with the *COSY*-based model for several EQS configurations. Measurements[6] – shown in arbitrary units – result from detections of minimum ionizing particles that deposit ~ 170 MeV of energy in two adjacent calorimeters within the ring while two collimators were inserted to the storage region.

field imperfections are treated as perturbations to the linear case. In particular, for simplicity this model assumes a smooth behavior of the unperturbed betatron oscillations that does resemble the real case:

$$x(\varphi) = H\cos(\nu_x\varphi)\,, \quad y(\varphi) = V\cos(\nu_y\varphi) \tag{2}$$

where φ is the azimuth and H and V are the radial and vertical betatron amplitudes, respectively. Considering both magnetic and electric potentials in the form

$$\Phi(x,y,\varphi) = \sum_{l=0}^{\infty}\sum_{m=0}^{\infty}\sum_{N=0}^{\infty} {}^{N}C_{l,m}x^l y^m\cos(N\varphi)\,, \tag{3}$$

we can combine Eq. 2 and Eq. 3 to estimate the transversal forces in terms of 2k-pole terms ($k = l + m$) and Nth azimuthal harmonics. The leading terms from Fourier analysis of the perturbations yield the following conditions that resonate with the betatron motion:

$$(l-1)\nu_x \pm m\nu_y \pm N = \Lambda\,, \quad l\nu_x \pm (m-1)\nu_y \pm N = \Lambda \tag{4}$$

where $\Lambda = \pm\nu_{x,y}$ depending on the field that drives the resonance. In general, vertical forces induce more muon losses than horizontal forces due to the relatively smaller vertical acceptance of the ring. The storage ring is four-fold symmetric, thus favoring $N = 0, 4, 8, \ldots$. Figure 7 depicts resonance lines as well as the operating set points of the storage ring. Resonant tune lines up to $k = 10$ are shown, which are sufficient for our purposes of covering all the main multipole terms that are implemented in the *COSY*-based ring model.

Along with the resonance conditions shown in Fig. 7, the observed resonances in the storage ring depend on the angle advancement spread in phase-space, betatron

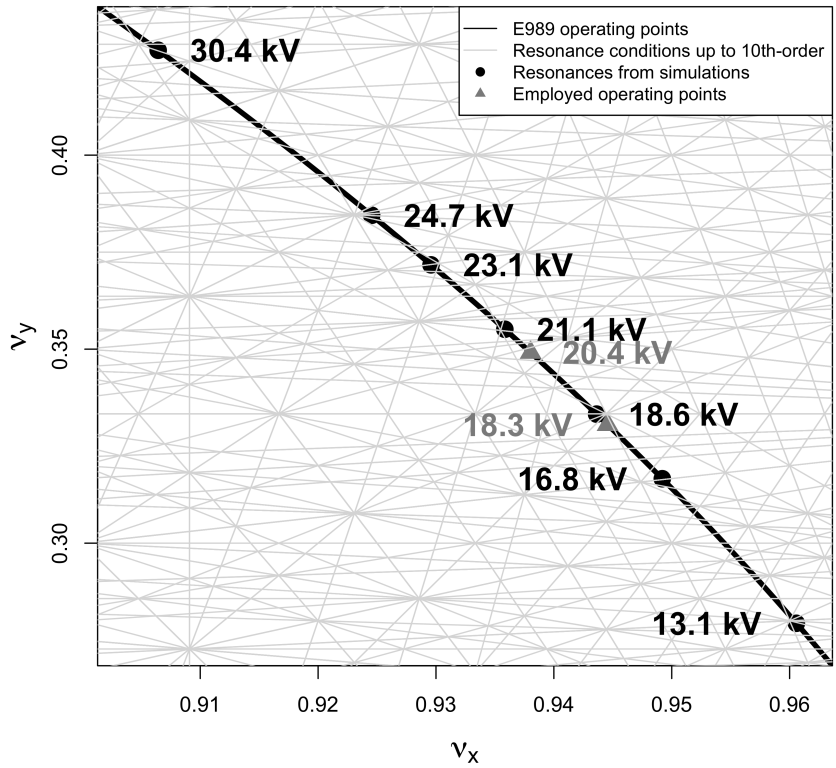

Fig. 7. An illustration of resonant tune lines and operating points of the g-2 storage ring. The high-voltage applied to the EQS plates to set operating points are shown next to resonances predicted by numerical studies with the *COSY*-based ring model. Measurements of lost muons have revealed resonance peaks at $\sim 13.1, 16.8, 18.6,$ and 21.1 kV as well (see Fig. 6). Lost muons measurements have not been performed for higher EQS voltages. Triangular markers show some operating points used in 2018 runs.

amplitudes, momentum, and initial phase of muons revolving the storage ring. The combination of these properties dictates how frequently a muon traverses unstable conditions in phase-space to undergo resonance or not. For instance, the continual growth of resonance peak widths for increasing HV's observed in Fig. 6 relates to the vertical angle advancement spread. This angle, which can be defined as the turn-by-turn angular evolution of the muon coordinates in vertical phase-space at an arbitrary azimuth location, advances in a more periodic manner as the vertical betatron function of the storage ring, β_y, significantly decreases on average for higher voltages within the explored HV range. Regarding betatron amplitudes and momenta, these properties – unique to each muon within the stored beam – could

also indirectly define the attributes of the peaks presented in Fig. 6 in that resonance conditions in Eq. 4 are not uniquely satisfied due to characteristic high-order tune shifts of the storage ring.[14]

To minimize systematic errors due to muon losses, the storage ring should run at operating points away from betatron resonances. As shown in Fig. 7, the system falls into resonance around specific set points and not at every intersection with resonant tune lines. This is mostly due to the rather specific set of nonlinear electrostatic $\phi(l, m)$ multipoles provided by the EQS, where the 20-th pole has the largest strength. Nevertheless, even though the multipoles that describe the measured magnetic field imperfections do not favor particular azimuthal harmonics due to their somewhat random distribution along the ring azimuth, they do have an important effect on betatron resonances as shown next.

3.2. *Muon Loss Driving Terms*

A deep understanding of the forces that drive betatron resonances is tantamount to a detailed characterization of the conditions in the storage ring that excite muon loss rates. By identifying all the resonances that emerge from the imperfections of the ring already known (i.e. nonlinear electric perturbations contributed by the EQS and magnetic field inhomogeneities from NMR probes measurements), it is possible to address the origin of resonant peaks from lost muons measurements not predicted by simulations. Extra peaks could be generated by mis-powering or misalignments of the EQS plates; transient magnetic fields outside the bandwidth of the NMR probes; and other factors not included in the *COSY*-based ring model that otherwise would be difficult to evaluate and would also directly affect the evolution of ω_a.

In addition, modifications to the default settings of the simulated ring model permit determining the driving terms that generate each betatron resonance peak. In Fig. 8, simulation results are shown for the following modifications to the original ring model configuration described in Sec. 2 (see markers' legend in Fig. 8 for each case):

(i) All E-multipoles, B-field inhomogeneities ON (original case, red)
(ii) Only 4th E-multipole, B-field inhomogeneities ON (gold)
(iii) No 20th E-multipole, B-field inhomogeneities ON (magenta)
(iv) All E-multipoles, B-field inhomogeneities OFF (blue)
(v) Only 4th and 20th E-multipoles, B-field inhomogeneities OFF (green)
(vi) No 20th E-multipole, B-field inhomogeneities OFF (orange).

The 2D multipole fits to the magnetic field NMR measurements (abbreviated as "B-field inhomogeneities" in the list above) introduce lost muon fractions of $\sim 6 \times 10^{-4}/\gamma\tau_\mu$ even at operating points away from the main betatron excitations. Some of the betatron resonance peaks observed from measurements and/or simulations (i.e. EQS plates voltage "*HV*" at $\sim 16.8, 21.1,$ and 24.7 kV) are fully explained from resonance conditions (Eq. 4) which can be independently driven by one or several

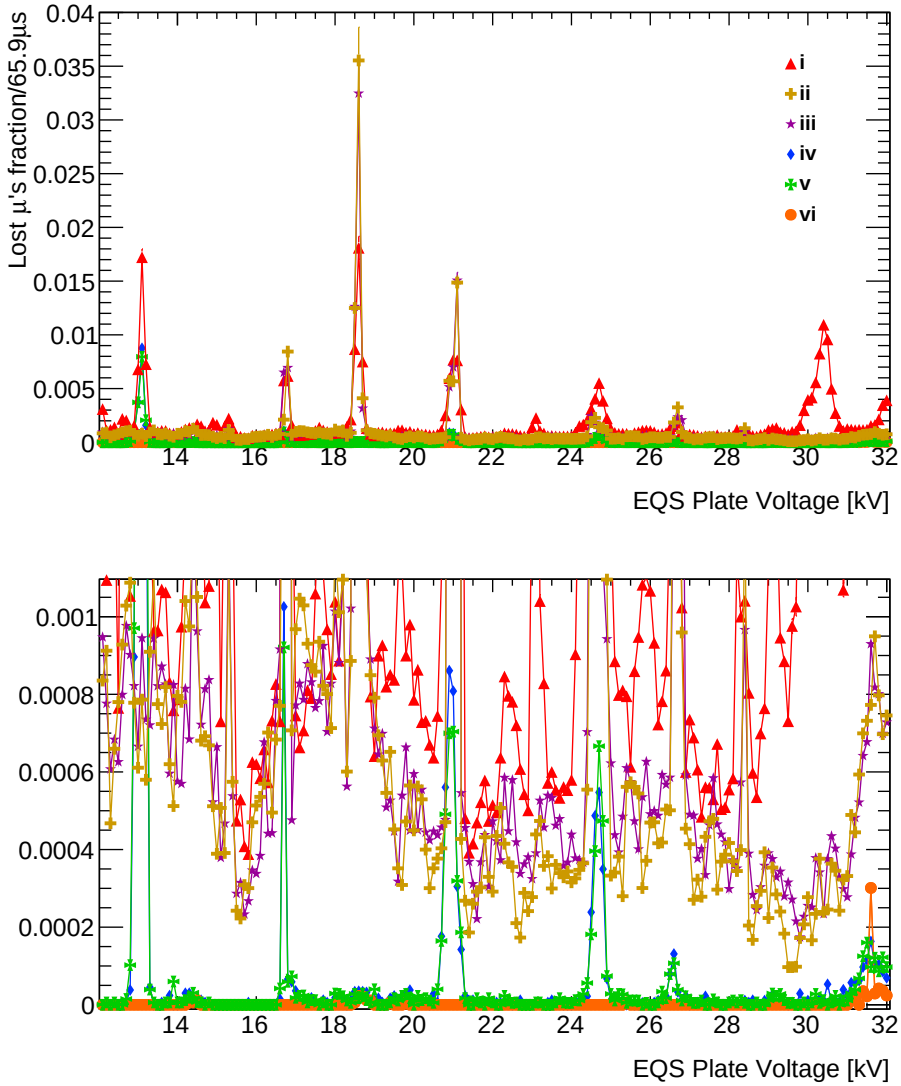

Fig. 8. Fraction of muon losses from simulations during the time interval $121 - 186\mu$s after beam injection. Configuration details are listed in Subsection 3.2. The bottom figure depicts lost muon fractions with a reduced vertical range to discern losses when magnetic field imperfections are not accounted for.

electric and magnetic high order multipoles in the storage ring model (see Table 2).

Nevertheless, Fig. 8 shows the interplay between magnetic(electric) nonlinearities and electric(magnetic) resonances. For instance, for a ring with $HV \sim 13.1$ kV the resonance driven by the electric ${}^{7}C_{7,3}$ and ${}^{7}C_{8,2}$ 20th-pole terms is boosted by

Table 2. Resonant conditions directly related to betatron excitations.

HV[kV]	$a\nu_x + b\nu_y = c$
16.8	$\nu_x - 3\nu_y = 0$
21.1	$\nu_x + 3\nu_y = 2$
24.7	$-\nu_x + 5\nu_y = 1 \quad , \quad 2\nu_x + 3\nu_y = 3$

lower order nonlinearities from the imperfect magnetic field; there are no resonant tune lines near such an operating point that could explain this effect with the guide fields set in simulations. However, by analyzing the high order terms of the storage ring transfer map in Normal Form (NF) it is possible to understand with more detail the role of nonlinearities in relation to resonances (see Refs. 12 and 14 for more details).

A similar occurrence of the reciprocity between resonances and nonlinearities from different origin, i.e. electric or magnetic, at $HV = 18.6$ kV is led by the electric 20th-pole, which in this case damps the resonance driven by magnetic multipoles that satisfy the resonant condition $3\nu_y = 1$. Furthermore, the $HV = 18.6$ kV peak is purely driven by the low order magnetic field multipoles as shown in Fig. 8.

NF methods also readily describe the negative reciprocity between the electric 20th-pole and multipoles from the magnetic field nonlinearities at $HV = 30.4$ kV. These resonance mechanisms are also of importance to address spin resonances, which could reduce the muon beam polarization depending on the operating point.

4. Conclusion

The detailed *COSY*-based ring model enabled to perform a quantitative analysis of betatron resonance peaks within the ring operating range in relation to the E989 systematic error from muon losses. Numerical results from simulations agree with current measurements, indicating a good performance of the ring computational model. After comparing stored and lost muons fractions away from excitation resonances, the optimal operating point that maximizes and minimizes those two fractions, respectively, corresponds to a voltage applied to the EQS plates around 28 kV. After this point, more regions without resonance conditions around exist; however, the electric horizontal defocusing from the EQS reduces the fraction of injected muons to the storage ring.

The understanding and characterization of lost muon resonances observed to date at E989 and presented above provide a basis to assess whether unexpected and difficult-to-measure imperfections manifest within the ring. Simulations identify the particular nonlinearities that could be addressed to reduce muon loss rates. Furthermore, regions of high muon losses at operating points of higher EQS voltages that the experiment pursues can be anticipated.

Even though driving terms were identified for all the betatron resonance peaks within the region examined in these studies, normal form methods provide a better understanding of the interplay between high and low order nonlinearities from the

measured/known imperfections of the electric and magnetic fields within the storage volume of the ring.

Acknowledgements

We are grateful to M. J. Syphers, W. M. Morse, A. Chapelain, P. Debevec, S. Ganguly, D. Stratakis, E. V. Valetov, and A. Weisskopf for valuable suggestions and discussions. In particular, the authors thank the following members of the Muon g-2 Collaboration at Fermilab for providing data that permitted to validate and produce the presented studies: H. Binney for the observed muon beam time profile; A. Chapelain for the experimental betatron tunes; J. D. Crnković for positron rate measurements; J. Grange and R. Osofsky for measurements of the storage ring magnetic field inhomogeneities; D. Rubin for a sample from simulations of the initial muon beam distribution properties; C. Stoughton for the kicker pulse pattern sample during initial runs; and L. Welty-Rieger for the storage ring layout. This work was supported by the U.S. Department of Energy under Contract No. DE-FG02-08ER41546 and Contract No. DE-SC0018636. This document was prepared using the resources of the Fermi National Accelerator Laboratory (Fermilab), a U.S. Department of Energy, Office of Science, HEP User Facility. Fermilab is managed by Fermi Research Alliance, LLC (FRA), acting under Contract No. DE-AC02-07CH11359. We are thankful to the PhD Accelerator Program at Fermilab and also for a Strategic Partnership Grant from the MSU Foundation. This research used resources of the National Energy Research Scientific Computing Center (NERSC), a U.S. Department of Energy Office of Science User Facility operated under Contract No. DE-AC02-05CH11231.

References

1. J. Grange *et al.*, "Muon g–2 Technical Design Report," Fermi National Accelerator Laboratory, Batavia, IL, USA, FERMILAB-FN-0992-E, Jan. 2015.
2. D. A. Tarazona *et al.,* "Realistic modeling of the Muon g-2 Experiment beamlines at Fermilab," *Proc. 13th Int. Computational Accelerator Physics Conf. (ICAP'18)*, Key West, USA, October 2018, paper MOPAF02, pp. 141–146.
3. K. Makino and M. Berz, "*COSY INFINITY* Version 9," *Nucl. Instr. Meth. A*, vol. 558, pp. 346–350, 2006.
4. M. Berz and K. Makino, "*COSY INFINITY* 10.0 Beam Physics Manual," Department of Physics and Astronomy, Michigan State University, East Lansing, MI, USA, Rep. MSUHEP–151103, Oct 2017.
5. G. W. Bennett *et al.* [Muon g-2 Collaboration], "Final report of the muon E821 anomalous magnetic moment measurement at BNL," *Phys. Rev. D* **73**, 072003 (2006).
6. Data provided by the Muon g-2 Collaboration at Fermilab.
7. D. Stratakis, M. E. Convery, C. Johnstone, J. Johnstone, J. P. Morgan, D. Still, J. D. Crnkovic, V. Tishchenko, W. M. Morse, and M. J. Syphers, " Accelerator performance analysis of the Fermilab muon campus," *Phys. Rev. Accel. Beams*, vol. 20, 111003, Nov 2017.
8. M. Korostelev *et al.,* "End-to-end beam simulations for the new Muon g-2 Experiment

at Fermilab," *Proc. 7th Int. Particle Accelerator Conf. (IPAC'16)*, Busan, Korea, May 2016, paper WEPMW001, pp. 2408–2411.
9. A. P. Schreckenberger *et al.*,"New Fast Kicker results from the Muon g-2 E-989 Experiment at Fermilab," *Proc. 9th Int. Particle Accelerator Conf. (IPAC'18)*, Vancouver, Canada, May 2018, paper THPML093, pp. 4879–4881.
10. Y. Semertzidis *et al.*, *Nucl. Instr. Meth. A* **503**, pp. 458–484, 2003.
11. E. V. Valetov and M. Berz,"Main and Fringe Field computations for the Electrostatic Quadrupoles of the Muon g-2 Experiment Storage Ring," *Proc. 13th Int. Computational Accelerator Physics Conf. (ICAP'18)*, Key West, USA, October 2018, paper TUPAG22, pp. 307–313.
12. M. Berz, *Modern Map Methods in Particle Beam Physics*, Advances in Imaging and Electron Physics, Vol. 108 (Academic Press, San Diego, 1999).
13. J. D. Crnkovic *et al.*,"Commisioning the Muon g-2 Electrostatic Quadrupole System," *Proc. 9th Int. Particle Accelerator Conf. (IPAC'18)*, Vancouver, Canada, May 2018, paper WEPAF015, pp. 1848–1851.
14. A. Weisskopf, D. A. Tarazona and M. Berz,"Computation and consequences of high-order amplitude and momentum dependent tune shifts in storage rings for high precision measurements," *Proc. 10th Int. Charged Particle Optics Conf. (CPO-10)*, Key West, USA, October 2018, this volume.